Energy 113 (2016) 852–860

Contents lists available at ScienceDirect

Energy

journal homepage: www.elsevier.com/locate/energy

Experimental and numerical investigation of core cooling of Li-ion cells using heat pipes

K. Shah, C. McKee, D. Chalise, A. Jain*

Mechanical and Aerospace Engineering Department, University of Texas at Arlington, USA

ARTICLE INFO

Article history:
Received 14 January 2016
Received in revised form
20 May 2016
Accepted 15 July 2016

Keywords:
Lithium-ion cells
Thermal runaway
Convective cooling
Heat pipe
Thermal management

ABSTRACT

While Li-ion cells offer excellent energy conversion and storage capabilities for multiple applications, including electric vehicles, heat removal from a Li-ion cell remains a serious technological challenge that directly limits performance, and poses serious safety concerns. Due to poor thermal conductivity of Li-ion cells, traditional cooling methods like air cooling on the cell surface do not effectively access and cool the core. This may lead to overheating of the cell core. This paper investigates the cooling of Li-ion cells using an annular channel through the axis of the cell. Air flow through this channel and heat pipe insertion are both shown to result in effective cooling. A temperature reduction of 18–20 °C in the cell core is observed in heat pipe experiments, depending on heat pipe size, for 1.62 W heat dissipation. Similar effect is observed when a thin metal rod is used instead of a heat pipe. Experimental measurements are close to finite-element simulation results. Experiments demonstrate that a heat pipe successfully prevents overheating in case of sudden increase in heat generation due to malfunction such as cell shorting. This paper illustrates fundamental thermal-electrochemical trade-offs, and facilitates the development of novel and effective cooling techniques for Li-ion cells.

1. Introduction

Lithium-ion cells offer excellent energy conversion and storage for a variety of applications, including consumer electronics, electric vehicles and military electronics [1,2]. Despite the excellent electrochemical characteristics of Li-ion cells compared to alternate energy storage and conversion technologies [3,4], the application of Li-ion cells has been severely limited by concerns over overheating during operation [5–8]. A significant amount of heat is generated, particularly at high discharge rates [9], and the poor thermal conductivity of Li-ion cells [10] results in large temperature rise within the cell [11,12]. Besides reduced performance and reliability at high temperatures, this also presents a serious safety concern [5,9]. Once the cell temperature exceeds a certain threshold, a series of exothermic processes occur within a Li-ion cell [13,14]. This thermal runaway situation eventually results in catastrophic failure and fire that may have led to several well-publicized recent incidents [6]. Several other undesirable effects, including capacity fade [15,16], power fade [5] and self-discharge [17] are also known at high temperature. Due to the importance of thermal management in a Li-ion cell, a variety of approaches for cell cooling have been investigated. The use of a heat pipe with a metal fin has been found to be effective for heat dissipation [18]. Analysis of convective cooling with air or liquid flow over the cell has been presented [19]. Phase change cooling has been shown to provide better heat dissipation than air cooling in certain conditions [20]. The role of phase change cooling on prevention of thermal runaway has been investigated [21]. The use of heat pipes distributed between cells has been shown to limit temperature rise [22].

The operation of a Li-ion cell depends on a complicated, multiscale coupling between several physical processes including charge/ion transport, electrochemistry, heat transfer, etc. [23–25]. Heat generation in a Li-ion cell is an undesirable side effect of the primary electrochemical energy conversion and storage function of the cell. Heat generation occurs due to a variety of mechanisms, including Ohmic losses, exothermic heats of reaction, etc. Theoretical analysis of these processes [26,27], as well as measurement of heat generation rates, have been presented in the past. This includes measurements at very high rates of discharge, using calorimetry [28] and measurement of heat stored and lost [9]. Due to the tight winding of the electrode-separator roll in a Li-ion cell, it is reasonable to assume that heat generation within a Li-ion cell is

* Corresponding author. 500 W First St, Rm 211, Arlington, TX, 76019, USA.
E-mail address: jaina@uta.edu (A. Jain).

http://dx.doi.org/10.1016/j.energy.2016.07.076
0360-5442/

spatially uniform, except possibly for greater heat generation at the tabs due to Ohmic losses. However, due to the relative proximity of the outer parts of a cell to a heat transfer path offered by air cooling or cold plate cooling, the outer parts of a cell cool down much more effectively than the core of the cell. Such approaches do not sufficiently address heat removal from the core of the cell, which remains thermally difficult to access.

Fundamentally, heat removal from a Li-ion cell is a two-step process – heat generated inside the cell is first conducted to the outside surface of the cell, followed by heat removal from the surface [11]. The second step of this process occurs typically through convection with a coolant, such as air, or conduction through the surrounding material of the battery pack. It has been shown that thermal conduction within the Li-ion cell is usually the slower, and hence rate-determining step [11]. This emanates from the poor thermal conductivity of the Li-ion cell, particularly in the direction normal to the electrodes [29]. This makes it particularly difficult to remove heat generated in the core of the cell, resulting in a hot core and a large temperature gradient within the cell. Measurements have shown as much as 24 °C temperature gradient between the core and outer surface of a 26650 cell at 10C discharge rate [9]. In addition, this results in a large temperature gradient within the cell based on both estimates [30] and actual measurements [31], which is undesirable for performance and reliability.

It is clearly important to remove heat directly from the core of the cell. Merely enhancing heat transfer on the outside surface, for example by increasing the coolant flowrate or improving cold plate design does not sufficiently enhance the cooling of the core of the cell, and may actually worsen the temperature gradient. In order to effectively cool the core of the cell, it is critical to thermally access the cell core and remove heat directly from the source of heat generation. A hollow metal tube that may be inserted along the axis of the cell during the electrode roll winding and assembly process may offer a mechanism for this purpose, for example, through the insertion of a heat pipe in the annular region. Heat pipes are passive devices that facilitate directional heat transport through evaporation and condensation of an enclosed working fluid in a spatial loop. Heat pipes have been widely used in several other applications, including electronic devices such as RF power device [32], microprocessors [33]. insulated-gate bipolar transistors (IGBTs) [34], data centers [35], photovoltaic cells for energy conversion [36] and district heating applications [37], high power LEDs [38], thermal energy storage [39], etc. but not so much for Li-ion cells. Some work has been recently reported on inserting heat pipes between cells in a pack without [22] and with heat spreaders [40]. There may be several technical challenges in the use of heat pipes, such as integration with present manufacturing processes, interference with electrical conductors and heat removal from the condenser end of the heat pipe. Further, the previously adopted approach of embedding a heat pipe between Li-ion cells has limited benefit as it does not access the core source of heat generation within the cell. It would be a lot more effective if the heat pipe can be inserted into the cell, since this would give a direct heat transfer pathway for the heat generated inside the cell to be dissipated. Due to the poor thermal conductivity, and hence large thermal resistance of materials inside a Li-ion cell, such a direct approach is expected to be a lot more effective than what has been investigated so far.

This paper investigates the thermal management of a Li-ion cell utilizing cooling through a hollow tube passing through the cell. The effectiveness of cooling a thermal test cell through internal air flow, as well as heat pipe and metal rod insertion is experimentally investigated. A thermal test cell of the same dimensions as a 26650 Li-ion cell, and similar thermal properties is fabricated. Heat generation in the test cell through Joule heating is used to mimic electrochemical heating in a Li-ion cell. Experimental data are shown to be in good agreement with finite-element simulation results. This approach is shown to result in effective cooling of the Li-ion cell due to the direct access provided to the core of the cell. Despite the several manufacturing challenges and thermal-electrochemical trade-offs that an embedded heat pipe may present, the dramatic improvement in thermal management may make this an attractive approach for thermal management of Li-ion cells.

The next section discusses fabrication of the thermal test cell, experimental setup and thermal measurements. Finite-element simulations are described next, followed by a discussion of key results and conclusions.

2. Experimental approach

2.1. Fabrication of annular thermal test cell

Electrochemical heat generation rate in a Li-ion cell varies as a function of the depth of discharge [31], and is difficult to measure directly [9]. Moreover, it is also not straightforward to measure temperature inside a Li-ion cell because a Li-ion cell is a hermetically sealed system, and drilling a hole to insert a thermocouple will disrupt the electrochemical function of the cell. As an alternative, a thermal test cell capable of precise, well-controlled heat generation through Joule heating and internal temperature measurement through embedded thermocouples is fabricated. This allows precise thermal measurements at well-controlled and measurable heat generation rates corresponding to discharge at various C-rates without the added uncertainty due to the electrochemistry of an actual Li-ion cell. The thermal test cell is designed and fabricated to be the same dimensions as a 26650 cell, and the constituent materials are chosen in order to closely match the thermal transport properties of an actual Li-ion cell [10,41].

Two thermal test cells with inner diameter of 2 mm and 6 mm are fabricated. A steel tube is first cut to approximately 110 mm in length. The outer surface of the tube is insulated with Kapton tape to prevent short circuiting. Next, a 25 μm thick stainless steel foil is cut 1000 mm long and approximately 62.5 mm wide. One side of this foil is insulated with Kapton tape to prevent the foil from short circuiting itself. Two 16 gauge wires are soldered to opposite ends of the foil for connecting to a power source. Seven T-type thermocouples are then placed at increasing distances from one another along the foil (Fig. 1a). The foil is then wrapped around the steel tube as tightly as possible in order to increase total heater length and hence electrical resistance. Once tightly wound, the roll is secured with tape (Fig. 1b). The tube and metal sheet roll are then placed inside the casing of a 26650 cell, and a thermocouple is also attached to the inside of the cell casing (Fig. 1c). The cell is filled with poly-dimethylsiloxane (PDMS), which is a thermally-curable polymer that fills up air voids within the test cell. Also, an additional ninth thermocouple is placed within the small layer of PDMS in between the foil and casing. All wires are threaded through a cap that is then inserted at the open end of the cell. PDMS inside the cell is cured at room temperature over a 24 h period. Since uncured PDMS is very viscous, in order to fully remove air bubbles, PDMS is topped off and self-cured once more.

Fig. 1d shows a top view image of the thermal test cell before sealing the top cap, showing the tightly wound metal heater coil and wires leading to the embedded thermocouples. The room temperature resistance of the heater coil is found to be 0.23 Ohms and 0.27 Ohms respectively for the heaters for the 6 mm and 2 mm hole diameter test cells, which was measured in a four-wire configuration due to the small value of the resistance. Resistance

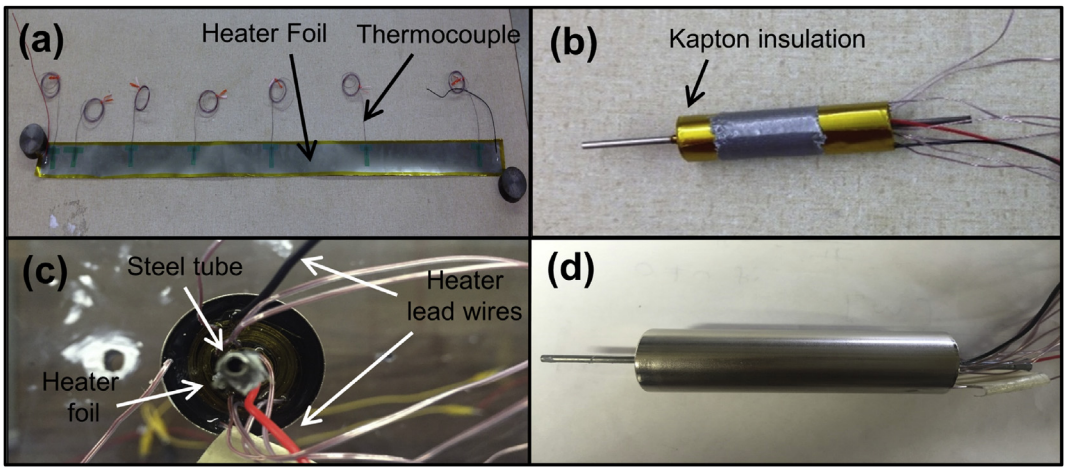

Fig. 1. Annular thermal test cell fabrication process.

is found to be largely independent of temperature in the temperature range of interest due to the low temperature coefficient of resistance of the heater material.

2.2. Thermal property measurement of thermal test cell

Experiments are carried out to measure the key thermal transport properties of the thermal test cell, to ensure that these values are close to that of a Li-ion cell [9,41]. Due to the spirally wound nature of the thermal test cell, similar to a 26650 Li-ion cell, a strong thermal conductivity anisotropy is expected, with radial thermal conductivity being much lower than the axial thermal conductivity. As a result, it is important to measure and characterize this rate-determining thermal property. This measurement is carried out by inserting a cartridge heater into the metal tubing of the test cell as shown in Fig. 2. A T-type thermocouple is also placed on the outer surface of the test cell. The cartridge heater spans the entire length of the cell, ensuring uniform heating. The test cell is oriented horizontally in order to minimize heat loss through conduction from the axial ends. A heating current of 58 mA is passed through the heater using a Keithley sourcemeter 2401, resulting in 1.21 W J heating. Temperature measured by the outside thermocouple as well as those embedded in the thermal test cell are logged at 2 Hz frequency using a National Instruments DAQ 9213. Experiments are carried out in two different ambient conditions, until steady-state conditions are reached, defined as less than a 0.5 °C temperature change over 600 s. Steady-state temperature data are then analyzed and compared with a one dimensional model for heat flow through an annular radial geometry with heat flux at the inner radius to determine the radial thermal conductivity of the thermal test cell.

Heat capacity of the test cell is determined by the mass-weighted average of the components used in fabricating the cell as follows:

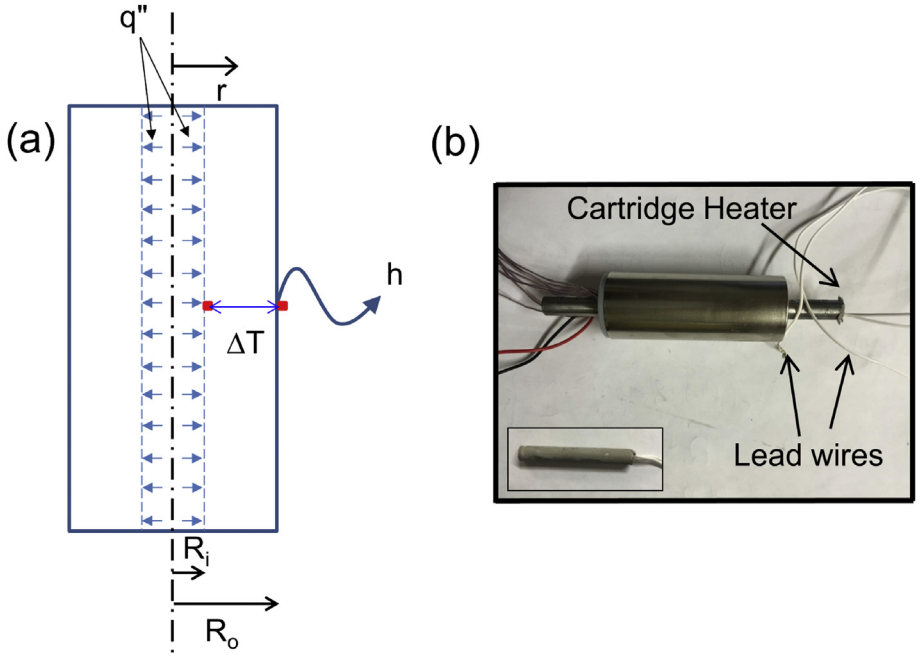

Fig. 2. (a) Picture of radial thermal conductivity measurement setup, (b) Schematic of heater and thermocouple locations for k_r measurement.

$$C_p = \frac{\sum_{i=1}^{N} m_i C_{p,i}}{\sum_{i=1}^{N} m_i} \quad (1)$$

where m and C_p refer to mass and heat capacity respectively, and the summations take place over all constituent materials.

Unlike thermal conductivity, heat capacity is a scalar quantity which at this length scale is given accurately by the mass-weighted average of heat capacities of constituent materials [42]. All materials used in fabricating the test cell are standard, with well-known thermal properties.

2.3. Experimental setup for thermal measurements

Experiments are carried out to investigate the thermal effectiveness of annular cooling of the thermal test cell. In the first set of experiments, the effect of coolant air passing through the annular tube is investigated. The cell is suspended in a low speed wind tunnel by connecting flexible piping on either end of the metal tube inserted into the test cell. Flow rate and pressure of air flow through the cell are controlled and measured using a ball valve, flowmeter and pressure gauge. The pressure gauge used is an Ashcroft 1226 commercial pressure gauge which has an accuracy of ±3% of its/full scale that is 100 kPa. Two different flow meters by King Instrument Company are used. One of them has a range of 6-60 SCFH (standard cubic feet per hour). The resolution of this flowmeter is 2 SCFH and the accuracy is ±3.6 SCFH. The other flow meter has a range of 0.8 SCFM-8.2SCFM (standard cubic feet per minute), a resolution of 0.2 SCFM and an accuracy of ±0.328SCFM. The volumetrically uniform heat is generated inside the cell by passing a heating current through the rolled metal foil in the test cell. A GPD-4303S programmable multichannel sourcemeter is used for this purpose. The sourcemeter has a current range of 0–3 A and voltage range of 0–30 V. It has an accuracy of ± (0.2% of the set value+3 mA). T-type thermocouples with an accuracy of 1 °C are embedded in the test cell are connected to a National Instruments DAQ 9213 for data acquisition. A number of experiments are carried out at various air flow rates, including a baseline experiment without any air flow. This experimental setup also enables the characterization of external cooling of the cell, where the airflow is directed over the cell instead of through the cell.

In the second set of experiments, passive cooling of the cell is investigated. A heat pipe is inserted into the metal tubing such that it can acquire heat from the entire length of the cell. Two Copper heat pipes of 2 mm and 6 mm diameter are used in these experiments. Each heat pipe is 10 cm in length. A test cell with a 2 mm heat pipe is shown in Fig. 3a. The test cell is suspended from the top wall of the wind tunnel in such a way that the condenser end of heat pipe that allows heat loss to the ambient protrudes out of the wind tunnel (Fig. 3b). A STANLEY High Velocity Blower Fan Model 655704 is placed outside the wind tunnel convects heat away from the condenser tip of the heat pipe. The airspeed from this air blower is measured using an Extech mini thermo-anemometer. The anemometer can measure air speed from 0.5 to 28 m/s with a resolution of 0.1 m/s. The accuracy of the air speed measured is ± (3% reading + 0.2 m/s). The air speed obtained from the blower is in the range of 0–8.4 m/s. For further investigation of this approach, experiments are also carried out where the heat pipe is replaced by a copper rod of the same size.

The test cell is subjected to internal heat generation through Joule heating. Measurements are carried out in two ambient conditions – natural convection where the condenser tip of the heat pipe cools off by itself, and forced convection where an external air flow occurs over the heat pipe tip. In the latter case, the physical isolation of the test cell from the air flow ensures that the external air flow cools the heat pipe tip, and not the cell directly.

3. Finite-element simulations

A finite element model is developed in ANSYS CFX [43] to model the experiments. The geometry of experimental test cells is modeled. The thermal conductivity of the cell is treated as anisotropic, with a radial thermal conductivity value of $k_r = 0.25$ W/mK, obtained from measurements as discussed in section 2.3. The value of uniform heat generation applied in the volume of the cell is taken to match experimental conditions. Appropriate fluid domains are also created for both the cooling cases. The geometry is meshed with over 1 million nodes, and grid independence checks are carried out.

For heat pipe based passive cooling, the heat pipe geometry is designed such that similar to experimental conditions, one end protrudes out of the test cell and other end stays within. A fluid domain is created to simulate air flow over the heat pipe in the case of forced convection. Inlet air velocity is assigned to one of the sides of the fluid domain to represent the air blower supplying cooling air stream over the heat pipe tip. A convective heat transfer coefficient of 10 W/m^{2}K is assigned to outer surfaces of the test cell, which is a typical value for natural convection conditions [44]. The effective thermal conductivity of the heat pipe is assumed to be 5000 W/mK. While the operation of a heat pipe is considerably complicated, involving fluid flow, phase change, etc., these phenomena result in a very high effective thermal conductivity that has often been used to simplify the modeling of a heat pipe [45].

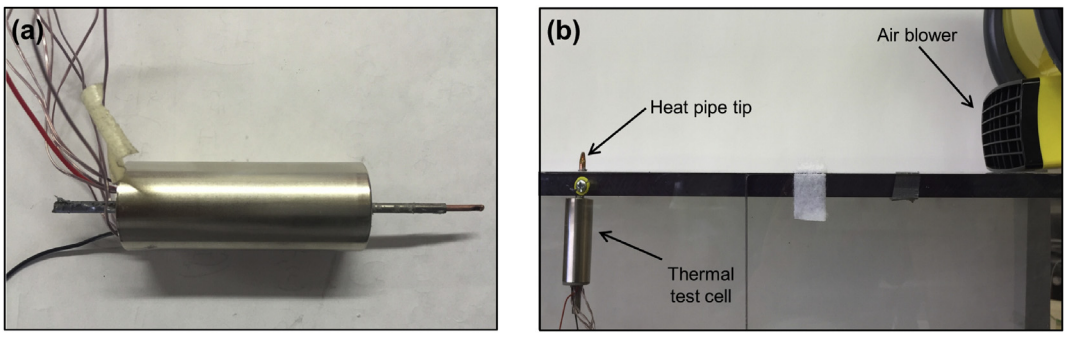

Fig. 3. Pictures of experimental setup: (a) Wind tunnel experimental setup for studying heat pipe-based cooling, (b) Thermal test cell with heat pipe inserted in the annular region.

4. Results and discussion

4.1. Thermal property measurement results

Thermal conductivity in the radial direction is a key thermal transport property of a Li-ion cell [10,11]. Due to the poor thermal properties of separator [46] and multiple thermal contact resistances in the rolled nature of the thermal test cell, similar to a Li-ion cell [29], the radial thermal conductivity k_r is expected to be much smaller than the axial component k_z, and hence likely to be the rate-determining thermal parameter. Experiments are carried out to determine the value of k_r as described in section 2.2. Considering an annular cylinder being heated on the inner surface and convectively cooled on the outer surface, the steady-state temperature distribution within the cylinder is given by

$$T(r) = \frac{q'' \cdot R_1}{k_r} \ln\left(\frac{R_1}{r}\right) + \frac{q''}{h}\frac{R_1}{R_2} \tag{2}$$

where k_r is the radial thermal conductivity and h is the convective heat transfer coefficient on the outside surface. q'' is the heat flux at the inner surface. R_1 and R_2 are inner and outer radii respectively. Note that in this case, temperature is not a function of the axial dimension z, since the cartridge heater supplies heat all along the z-axis. From equation (2), the temperature difference between the inner and outer surfaces is given by

$$\Delta T = T(R_1) - T(R_2) = \frac{q'' \cdot R_1}{k_r} \ln\left(\frac{R_2}{R_1}\right) \tag{3}$$

Equation (3) shows that the steady-state temperature difference between thermocouples mounted on the inner and outer surfaces can be used to determine the radial thermal conductivity, since q'', R_1 and R_2 are well-known.

Experiments are carried out in two different ambient conditions – free convective cooling of the thermal test cell, and forced convective cooling due to a stream of cooling air directed at the test cell. The measured temperature distribution within the cell is plotted in Fig. 4 for both cases. The temperature difference ΔT between the innermost and outermost thermocouples results in consistent determination of k_r from both experiments. As expected, the measured temperature difference ΔT is nearly the same in both ambient conditions, resulting in thermal conductivity values of 0.25 W/mK and 0.26 W/mK in free and forced convection respectively. These values are very close to the radial thermal conductivity of a 26650 Li-ion cell [10].

Further, equation (2) is used to determine the radial locations of the thermocouples by fitting the expected radial temperature distribution through the experimental data. This precisely determines the locations of the embedded thermocouples as shown in Fig. 4. For reference, the approximate thermocouple locations based on a top-view picture of the rolled thermal test cell prior to sealing the cell cap are also shown. In most cases, the experimentally determined locations are close to the approximate locations. While the thermocouples were distributed approximately uniformly during the rolling and assembly process of the test cell, some movement is likely, and these experiments help determine the precise locations of the thermocouples.

Once k_r has been determined, temperature measurement from the outer-most thermocouple can also be used to determine the value of the convective heat transfer coefficient h using equation (2). This value is found to be 15 W/m^{2}K and 591 W/m^{2}K for natural and forced convection respectively, both of which are well within the range for these convective cooling regimes [44].

Compared to k_r, the axial thermal conductivity k_z does not play a significant role in determining the thermal characteristics of the test cell, since k_z is typically much larger due to the availability of a high thermal conductivity pathway for axial heat transfer. Fig. 5 plots the temperature distribution inside a cell for a fixed heat generation rate and convective cooling conditions for a number of k_z values based on a recently reported analytical thermal model of an annular geometry [47]. This plot shows that the temperature distribution is largely insensitive to k_z. A value of $k_z = 30$ W/mK is assumed based on past measurements [10].

In addition to a close match in k_r between the thermal test cell and a 26650 Li-ion cell, the specific heat and mass density are also found to match closely. The specific heat of the test cell, determined using a weighted average of its constituent materials is found to be 777 J/kgK, which is close to a recently reported measurement of 749 J/kgK [41]. The mass density of the test cell is found to be 2093 kg/m^3, which is close to the value of 2285 kg/m^3 for a 26650 cell [10]. Overall, the thermal mass of the thermal test cell is 56 J/K, compared to 59 J/K for a 26650 Li-ion cell.

4.2. Internal cooling

A set of experiments are carried out to investigate the effect of internal flow through the annular tube of the thermal test cell on

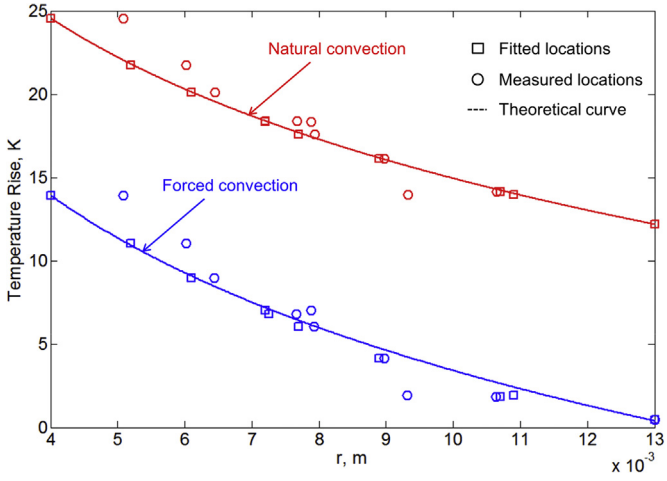

Fig. 4. Measured T vs r and analytical model fit for radial thermal conductivity measurement at two different convective conditions.

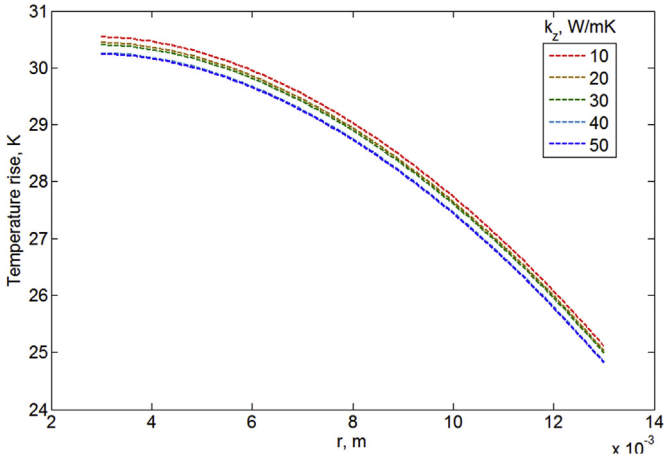

Fig. 5. T vs. r for a number of k_z values, showing weak dependence on axial thermal conductivity.

temperature distribution in the test cell with a heating current of 1.5 A. Data is obtained for cells with 2 mm and 6 mm diameter inner tubes. Fig. 6(a) and (b) present the measured temperature distribution for 2 mm and 6 mm cells respectively for a fixed heat generation rate of 1.62 W, but with different coolant flowrates. The presence of even a small coolant flowrate is shown to result in significant temperature reduction in comparison with the baseline case of no cooling. Specifically, the thermocouple closest to the core of the cell experiences the greatest temperature reduction – nearly 22 °C reduction with 1415 cm^3/s air flow, and the peak temperature rise shifts outwards within the cell. In comparison, temperature in the outer regions of the cell that are farthest from the coolant flow also reduces, but not as dramatically. The effect of the coolant flow saturates somewhat with increasing flowrate, most likely because thermal conduction within the cell begins to dominate the overall thermal transport process. For example, there is not much further reduction in temperature between 472 and 1415 cm^3/s measurements. This saturation effect is shown clearly in Fig. 7, which plots the peak temperature rise as a function of coolant flowrate for both 2 mm and 6 mm thermal test cells for 1.62 W heat generation rate. Fig. 7 shows that the thermal characteristics of the 2 mm and 6 mm cells with internal coolant flow are very similar to each other.

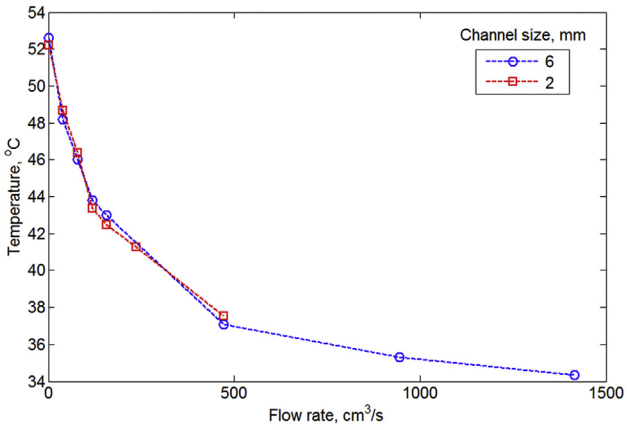

Fig. 7. Maximum cell temperature as a function of internal flowrate for 2 mm and 6 mm cells.

4.3. Heat pipe and metal rod cooling

Results from experiments with embedded heat pipes are summarized in Fig. 8, where the measured temperature distribution within the cell is plotted for a baseline case as well as with 2 mm (Figure 8a) and 6 mm (Fig. 8b) heat pipes. In each case, the cell dissipates 1.62 W heat. Two ambient conditions around the tip of the heat pipe are considered – one where the tip of the heat pipe loses heat simply by natural convection, and one where air flow over the top of the heat pipe (Fig. 3) results in greater heat loss due to forced convective cooling. In addition to heat pipes, Fig. 8(a) and (b) also show experimental data for the same power when a plain copper rod of the same size as the heat pipe is used instead. Data show significant reduction in temperature of the thermal test cell due to thermal transport from the core of the cell to the heat pipe. There is a reduction of 3 °C and 17 °C in peak temperature compared to baseline for natural and forced convection on the heat pipe respectively for the 6 mm case. These data show that while some temperature reduction is to be expected by simply embedding the heat pipe, an even greater benefit can be obtained when the tip of the heat pipe is cooled through forced convection. This is along expected lines, since forced convection ensures effective rejection of heat from the tip of the heat pipe into the ambient. In the absence of forced convection, heat flows from the cell into the heat pipe, but is severely impeded in transferring to the ambient, thereby reducing the overall heat transfer effectiveness of the heat pipe. The reduction in temperature for 1.62 W heat dissipation within the cell for 6 mm and 2 mm heat pipes is summarized in Fig. 9. Unlike flow-based cooling discussed in section 4.2, where thermal test cells with 2 mm and 6 mm inner tubes had similar thermal performance, in this case, there is greater temperature reduction when using a 6 mm heat pipe compared to a 2 mm heat pipe. However, a 6 mm heat pipe occupies greater volume inside the cell, and thus may result in reduced capacity compared to the 2 mm heat pipe cell. Data presented here helps quantify such thermal-electrochemical trade-offs in the thermal management of a Li-ion cell.

Data presented in Fig. 8(a) and (b) indicate that a cooling effect similar to a heat pipe may be obtained by simply using a copper rod instead of a heat pipe. In each case, the measured temperature distribution with a copper rod is very close to that with a heat pipe of the same size. Theoretically, this occurs because the thermal conductance through the metal rod is already so high that further increase in thermal conductance brought about by two-phase cooling within the heat pipe has negligible impact on the temperature field which is now dominated by thermal conduction within the cell and convection from the heat pipe or metal rod to

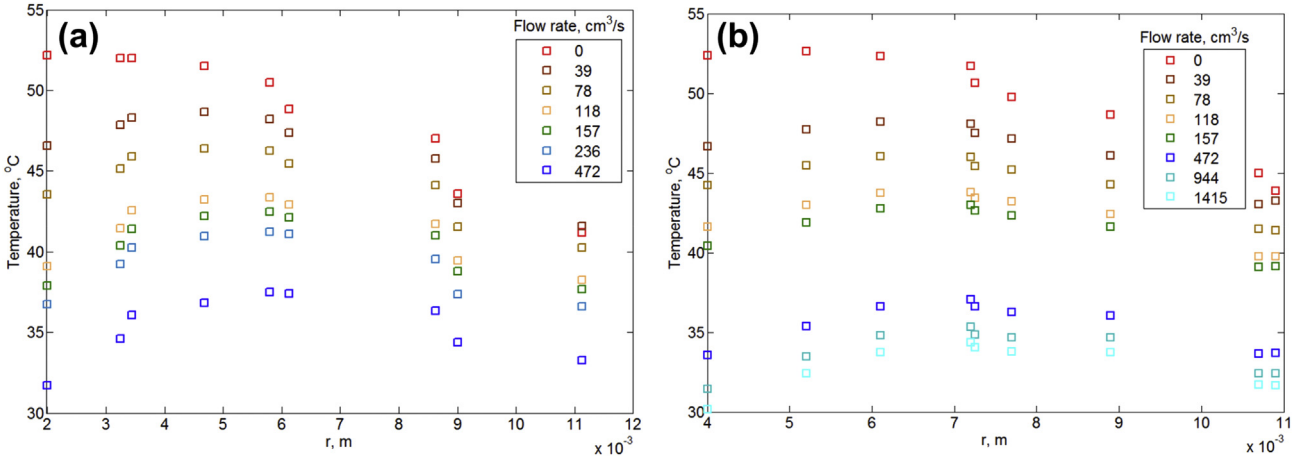

Fig. 6. Temperature distribution within the cell for baseline and several internal flowrates for (a) 2 mm cell, (b) 6 mm cell.

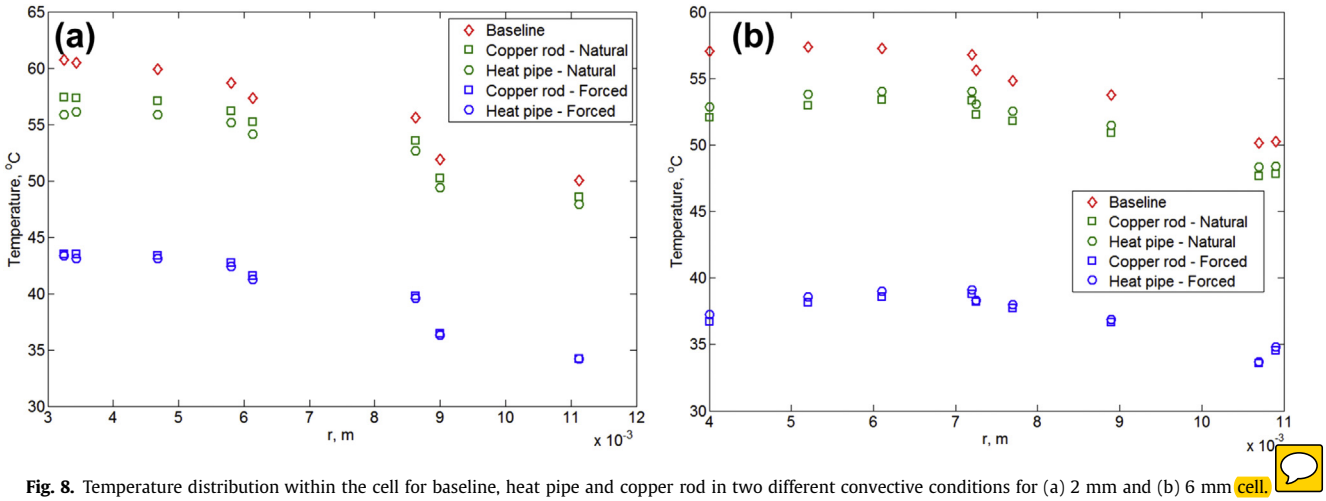

Fig. 8. Temperature distribution within the cell for baseline, heat pipe and copper rod in two different convective conditions for (a) 2 mm and (b) 6 mm cell.

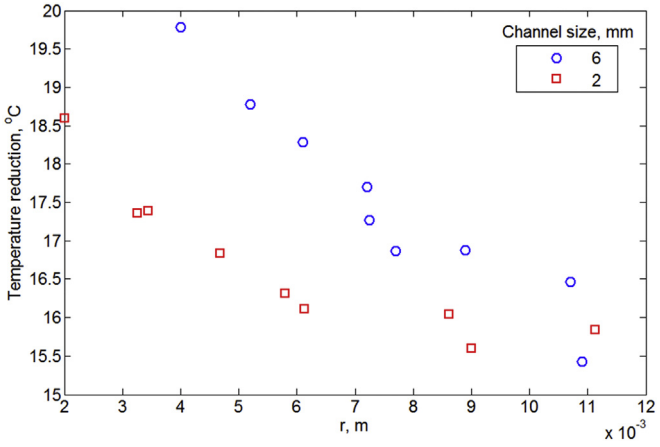

Fig. 9. Comparison of thermal performance of 2 mm and 6 mm heat pipes.

the ambient. Note that a metal rod is expected to be of much lower cost, since it does not require a hollow tube and various heat pipe components such as heat pipe fluid, wicking structure, etc. While 2 mm diameter copper rod can be obtained very easily and at low cost, a 2 mm diameter heat pipe can be prohibitively expensive.

In addition to reduced peak temperature, the presence of the heat pipe or metal rod improves temperature uniformity within the thermal test cell. As shown in Fig. 8(a) and (b), the temperature distribution is much flatter for both 2 mm and 6 mm cases compared to respective baselines, particularly when forced convection cooling is present.

Both heat pipe and metal rod, when embedded in the core of the cell as shown here provide a low thermal resistance path for heat generated in the cell to dissipate to the ambient. Despite a heat pipe being significantly more expensive than a metal rod, results presented here show that the thermal effect is similar in the two cases. In addition, while the 6 mm heat pipe shows better thermal performance than a 2 mm heat pipe, the 6 mm heat pipe occupies more space inside the cell, and thus may cause greater reduction in cell capacity for the same outer cell volume (around 20% reduction vs. 2% reduction based on volume).

Table 1 shows a comparison of experimentally measured temperature rise at the inner-most thermocouple in the cell with finite element simulation results. Results for a number of cooling conditions are listed, including the baseline case, air cooling cases and forced and natural convection cases for a heat pipe. There is good agreement between experiments measurements and simulations in each case. Note that similar to experiments, the simulations results predict that thermal performance of heat pipe and metal rod are close to each other. This is because in each case, thermal transport becomes limited by convection at the tip due to the comparatively lower thermal resistance within the heat pipe or metal rod. This may be an important consideration in the design of a thermal management technique for a Li-ion cell.

4.4. Effect of heat pipe cooling on anomalous heat generation

Experiments are also carried out to demonstrate the effect of the embedded heat pipe on the transient thermal response of the cell in realistic conditions. The cell is first subjected to a fixed heat generation rate, which is then increased four-folds. This may be representative of a situation where the cell experiences an anomalous increase in heat generation rate due to a malfunction such as an internal short. The thermal response of the cell is very critical in this situation, since thermal runaway may occur if the cell temperature exceeds a certain threshold. The presence of an embedded heat pipe may be able to prevent such a situation by directly removing the additional heat being generated in the core of the cell to the ambient. In order to quantify this, experiments are carried out without and with the embedded heat pipe. Results are summarized in Fig. 10, where the measured peak temperature

Table 1
Comparison of experimental measurements and simulation results for temperature rise at the inner wall in °C in various cooling cases.

	No cooling	Air cooling			Heat pipe or Cu rod	
		157 cm^3/s	236 cm^3/s	472 cm^3/s	Natural convection	Forced convection
Experimental measurement	52.4	33.6	31.4	30.2	52.1	36.7
Simulation result	53.5	33.0	30.9	30.1	48.8	38.3

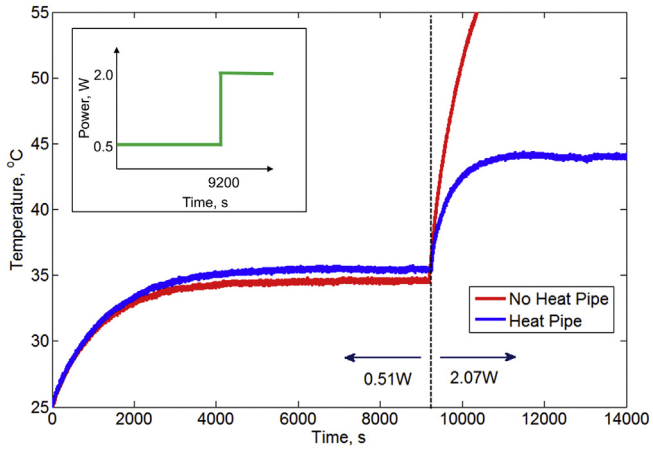

Fig. 10. Comparison of thermal performance without and with heat pipe during an anomalous heat generation event, showing preventing of overheating by the heat pipe.

is plotted as a function of time for both cases. Variation in the cell power with time is shown in the inset, and the time at which anomalous heat generation commences is indicated. When no heat pipe is present, the peak temperature in the cell starts increasing sharply as soon as the increased power is applied to the cell. The cell temperature rapidly reaches the threshold of 55 °C, at which point the experiment is terminated for safety of the cell. On the other hand, when a heat pipe is present, the temperature of the cell increases at a much lower rate, and eventually reaches a steady-state without exceeding the safety threshold. This shows that the heat pipe successfully prevents overheating of the cell, whereas without the heat pipe, the cell temperature rapidly reaches a threshold where it may be at risk of thermal runaway. This experiment highlights the potential thermal benefit of an embedded heat pipe in ensuring the safety of a cell during an anomalous heat generation event.

In each experimental dataset presented here, the experimental measurement uncertainty for temperature measurement is estimated to be 1 °C, based on thermocouple manufacturer specifications. Since temperature is measured directly, there is no other significant source of uncertainty in temperature measurement.

5. Conclusions

Thermal management of Li-ion cells is a critical technological challenge that directly affects the safety and reliability of Li-ion cells. Experiments carried out in this work indicate the promising nature of heat pipe based cooling. In particular, a heat pipe embedded in the core of the cell results in rapid dissipation of heat generated in the core, which is otherwise very difficult to access using other thermal management approaches. Experiments discussed here also show that the thermal performance of a heat pipe may be similar to that of a metal rod of the same size. An experiment mimicking a realistic cell failure shows the potential of an embedded heat pipe in delaying or preventing thermal runaway due to excessive heat generation in the cell.

The thermal benefits of core cooling demonstrated here must be considered along with the energy density loss due to the fabrication of the internal tube passing through the cell. Results here show that even a relatively small, 2 mm diameter tube that causes only 2% energy density loss can provide significant cooling effect. Increasing the inner diameter, while improving thermal performance somewhat also leads to more drastic energy density loss.

While there are several implementation challenges related to the integration of an embedded heat pipe in a Li-ion cell, the thermal benefits of this approach may justify the additional complexity during cell assembly. These manufacturing challenges must be explored further in the context of potential thermal benefits. Further, thermal-electrochemical tradeoffs involved in the implementation of heat pipe based cooling must be investigated.

Acknowledgments

This material is partly based upon work supported by CAREER Award No. CBET-1554183 from the National Science Foundation. Heat pipe assistance from Dr. Winston Zhang, Novark Technology Inc. is gratefully acknowledged.

References

[1] Scrosati B, Garche J. J Power Sources 2010;9:2419–30.
[2] Goodenough J, Park K-S. J Am Chem Soc 2013;135:1167–76.
[3] Linden D, Reddy TB. Handbook of batteries. third ed. New York: McGraw-Hill; 2002.
[4] Armand M, Tarascon J-M. Nature 2008;451:652–7.
[5] Bandhauer TM, Garimella S, Fuller T. J Electrochem Soc 2011;158:R1–25.
[6] Lisbona D, Snee T. Process Saf Env Prot 2011;89:434–42.
[7] Belov D, Yang M-H. J Solid State Electrochem 2008;12:885–94.
[8] Wang Q, Ping P, Zhao X, Chu G, Sun J, Chen C. J Power Sources 2012;208:210–24.
[9] Drake SJ, Martin M, Wetz DA, Ostanek JK, Miller SP, Heinzel JM, et al. J Power Sources 2015;285:266–73.
[10] Drake SJ, Wetz DA, Ostanek JK, Miller SP, Heinzel JM, Jain A. J Power Sources 2014;252:298–304.
[11] Shah K, Drake SJ, Wetz DA, Ostanek JK, Miller SP, Heinzel JM, et al. J Power Sources 2014;258:374–81.
[12] Shah K, Drake SJ, Wetz DA, Ostanek JK, Miller SP, Heinzel JM, et al. J Power Sources 2014;271:262–8.
[13] Spotnitz R, Franklin J. J Power Sources 2003;113:81.
[14] Abraham DP, Roth EP, Kostecki R, McCarthy K, MacLaren S, Doughty DH. J Power Sources 2006;161:648.
[15] Aurbach D, Markovsky B, Salitra G, Markevich E, Talyossef Y, Koltypin M, et al. J Power Sources 2007;165:491.
[16] Santhanagopalan S, Zhang Q, Kumaresan K, White RE. J Electrochem Soc 2008;155:A345–53.
[17] Johnson BA, White RE. J Power Sources 1998;70:48–54.
[18] Wu M, Liu KH, Wang Y, Wan C. L Power Sources 2002;109:160–6.
[19] Pesaran AA. Battery thermal management in EVs and HEVs: issues and solutions. In: Advanced automotive battery conference, Las Vegas, NV, USA; 2001.
[20] Sabbah R, Kizilel R, Selman JR, Al-Hallaj S. J Power Sources 2008;182:630–8.
[21] Kizilel R, Sabbah R, Selman JR, Al-Hallaj S. J Power Sources 2009;194:1105–12.
[22] Rao Z, Wang S, Wu M, Lin Z, Li F. Energy Convers Manag 2013;65:92–7.
[23] Bharathan D, Pesaran A, Vlahinos A, Kim G. Improving battery design with electro-thermal modeling. In: Proc. IEEE conf. Vehicle power and propulsion; 2005.
[24] Yi Y, Shi Y, Cai N, Lee J, He X. J Power Sources 2012;199:227–38.
[25] Srinivasan V, Wang CY. J Electrochem Soc 2003;150:A98–106.
[26] Thomas K, Newman J. J Power Sources 2003;119:844–9.
[27] Bernardi D, Pawlikowski E, Newman J. J Electrochem Soc 1985;132:5–12.
[28] Ye Y, Saw LH, Shi Y, Somasundaram K, Tay AAO. Electrochim Acta 2014;134:327–37.
[29] Vishwakarma V, Waghela C, Wei Z, Prasher R, Nagpure SC, Li J, et al. J Power Sources 2015;300:123–31.
[30] Lin X, Perez H, Siegel J, Stefanopoulou A, Li Y, Anderson R, et al. IEEE Trans Control Syst Technol 2013;21:1745–55.
[31] Forgez C, Do DV, Friedrich G, Morcrette M, Delacourt C. J Power Sources 2010;195:2961–8.
[32] Nelson LA, Sekhon KS, Fritz JE. 3rd international heat pipe conference, Vol. 1; 1978.
[33] Kim K, Won M, Kim J, Back B. Appl Therm Eng 2003;23:1137–44.
[34] Vasilieva L, Lossouarn D, Romestant C, Alexandre A, Bertin Y, Piatsiushyk Y, et al. Int J Heat Mass Transf 2009;52.1:301–8.
[35] Jouhara H, Meskimmon R. Energy 2014;77:265–70.
[36] Akbarzadeh A, Wadowski T. Appl Therm Eng 1996;16.1:81–7.
[37] Jouhara H, Milko J, Danielewicz J, Sayegh MA, Szulgowska-Zgrzywa M, Ramos JB, et al. Energy 2016. http://dx.doi.org/10.1016/j.energy.2016.04.070 [in press].
[38] Lu XY, Hua TC, Liu MJ, Cheng YX. Thermochim Acta 2006;493:25–9.
[39] Amini A, Miller J, Jouhara H. Energy 2016. http://dx.doi.org/10.1016/j.energy.2016.02.089 [in press].

[40] Ye Y, Saw LH, Shi Y, Tay AAO. Appl Therm Eng 2015;86:281–91.
[41] Zhang J, Wu B, Li Z, Huang J. J Power Sources 2014;259:106–16.
[42] Kaviany M. Principles of heat transfer. first ed. John Wiley & Sons; 2002.
[43] http://www.ansys.com/Products/Fluids/ANSYS-CFX, last accessed May 4, 2016.
[44] Incropera FP, Dewitt DP. Introduction to heat transfer. 3rd. Ed. Wiley Inc.; 2006.
[45] El-Nasr AA, El-Haggar SM. Heat Mass Transf 1996;32:97–101.
[46] Vishwakarma V, Jain A. J Power Sources 2014;272:378–85.
[47] Shah K, Jain A. Int J Energy Res 2015;39:573–84.